Dalton Transactions

ROYAL SOCIETY OF CHEMISTRY

PAPER

View Article Online
View Journal | View Issue

Cite this: *Dalton Trans.*, 2025, **54**, 17839

Structures and thermodynamics of dinuclear species formed in a uranyl(VI)–malic acid system: a multi-technique approach

Raúl Eduardo Linares-Jiménez, [a] Björn Drobot, [a] Robin Steudtner, [a] Satoru Tsushima, [a,b] Dominik Goldbach,[a] Thorsten Stumpf, [a] Susanne Sachs [a] and Jerome Kretzschmar *[a]

Although uranyl(VI)–malate systems have been repeatedly studied, there are still open questions regarding their structures, stoichiometry, and thermodynamic key parameters. We therefore examined the interactions between the uranyl(VI) ion, U(VI), and malic acid, H_2Mal, using a multi-technique approach performing nuclear magnetic resonance spectroscopy (NMR), time-resolved laser-induced fluorescence spectroscopy (TRLFS), isothermal titration calorimetry (ITC), and ultraviolet-visible spectroscopy (UV-vis), complemented by density functional theory (DFT) calculations. In acidic solution (pH 1.5–5.5), by covering metal excess through ligand excess, two dinuclear complexes of 2 : 1 and 2 : 2 U(VI) : malate stoichiometry form predominantly. This species distribution is mainly influenced by the metal-to-ligand ratio given in solution. DFT and NMR confirmed that the 2 : 1 U(VI) malate complex involves a bridging hydroxo ligand (μ_2-OH). In both the 2 : 1 and 2 : 2 complexes, malate features a (κ^3O,O′,O″) coordination motif with two carboxylate groups and the alkoxylato group including bridging between two U(VI). In the 2 : 2 complex, changing the ligands' relative orientation yields two geometric isomers. Thermodynamic quantities (ΔG, ΔH, and ΔS) and formation constants ($\log \beta$) of both complexes were determined by calorimetric titrations and TRLFS. The formation of the 2 : 1 and 2 : 2 species is endothermic and entropy-driven, with $\log \beta$ of 17.1 ± 0.1 and 37.7 ± 0.1, respectively. Notably, even for U(VI) concentrations as low as 10 μM, dinuclear species are predominant, while mononuclear species exist only in very acidic and/or very dilute solutions. This study provides new data which complement and expand the understanding of both structures and thermodynamics of these complexes.

Received 3rd September 2025,
Accepted 11th November 2025

DOI: 10.1039/d5dt02117k

rsc.li/dalton

Introduction

Malic acid (2-hydroxybutanedioic acid) is a hydroxydicarboxylic acid that appears as a metabolic intermediate of the tricarboxylic acid cycle in organisms with anaerobic and aerobic respiration.[1] It is one of the most abundant root exudates of plants along with citric and succinic acids. The secretion of malic acid has been observed to increase the tolerance of plants against aluminum and to support the release of inorganic phosphorus from minerals under phosphorus deficiency.[2–6] The increase of U(VI) mobility due to its complexation with malic acid was reported for plant cell cultures.[7] Plants secrete malic acid also as a signaling compound, for instance, after infection with foliar pathogens to serve as a recruitment signal for beneficial rhizobacteria[8,9] to stimulate the formation of beneficial biofilms[10] or to act as a chemo-attractant in the rhizosphere.[11]

Malic acid has two stereoisomers, the L- and D-isomers, with only the L-isomer occurring naturally in biological systems.[12] It has three functional groups, two carboxyl and one hydroxyl groups, with pK_a values of 3.4 and 5.1 for the carboxyl groups[13,14] and 14.5 for the hydroxyl group,[15] and will thus hereafter be denoted as H_2Mal. After consecutive deprotonation of the carboxyl groups, $HMal^-$ and Mal^{2-} are formed. As for other hydroxycarboxylic acids, deprotonation of hydroxyl groups in aqueous solution occurs only under extreme conditions. However, as will be of importance in the complexation studies, H^+ abstraction can be facilitated at much lower pH upon metal ion coordination (metal ion-promoted ligand deprotonation).[16–18] Given the similarity in structural features and hence pK_a values for the hydroxyl groups of citric acid and malic acid,[15] deprotonation of the hydroxyl group of Mal^{2-} during complexation with metal ions is anticipated and will be referred to as Mal_{-H}^{3-}.

[a]*Helmholtz-Zentrum Dresden-Rossendorf, Institute of Resource Ecology, Bautzner Landstraße 400, 01328 Dresden, Germany. E-mail: j.kretzschmar@hzdr.de*
[b]*Laboratory for Zero-Carbon Energy, Institute of Science Tokyo, Tokyo 152-8550, Japan*

Uranium (U) has a wide range of concentrations that can vary from 21.4 μg L^{-1} in surface waters to 749 μg L^{-1} in groundwater.[19] However, these natural amounts of U are increased by anthropogenic activities, such as U mining and milling, military use, and phosphate industry – including fertilizers. In the nuclear industry, U is used as fuel for electricity production in nuclear power plants. It is considered a contaminant of concern due to its toxicity to different organisms such as plants, animals, and microorganisms.[20–24] In humans, U has been observed to produce diseases in different tissues such as the brain, kidneys, liver, or lungs.[25–27] U exposure to humans mainly occurs from food and water uptake.[28,29] Although naturally occurring U has a low radiotoxicity, it shows a potent chemotoxicity.[27] Thus, knowledge of the interaction and transfer behavior of U in the environment up to the food chain is key in radioecology and pivotal for risk assessments of radioactive contaminated sites as well as for developing effective remediation strategies to prevent serious health hazards for humans.

Malic acid has been identified as a notable chelating agent for a broad variety of metal ions.[30–33] Therefore, interaction between U and H_2Mal is expected when both are present in soil environments. Complexation of uranyl(VI) and UO_2^{2+} with H_2Mal has already been the subject of several studies.[34–39] Rajan and Martell reported the uranyl(VI) malate complex to be dinuclear, where each malate ligand is fully deprotonated (Mal_{-H}^{3-}) and shared between two U(VI) ions.[36] Based on spectrophotometric studies in solution at pH 3.5, the formation of complexes having uranyl(VI) : malate ratios of 2 : 1 and 2 : 2 was suggested by Feldman and Havill.[39] Allen *et al.* determined the structural parameters of a 2 : 2 uranyl(VI) malate dimer in solution between pH 2 and 4 by means of extended X-ray absorption fine structure spectroscopy (EXAFS).[38] Only a limited number of studies have focused on the thermodynamic characterization of uranyl(VI) malate complexes. Feldman *et al.* reported on uranyl(VI) malate 2 : 2 dimers and 3 : 3 trimers.[34] Rajan and Martell expanded the set of species by proposing 1 : 1, 2 : 2, 3 : 3, and 6 : 6 uranyl(VI) malate complexes by potentiometry with 1 M KNO_3.[36] Kirishima *et al.* inferred the formation of 1 : 1 and 1 : 2 uranyl(VI) malate complexes with potentiometry and isothermal microcalorimetry in 1 M $NaClO_4$ at 25 °C.[40] Although previous studies have provided thermodynamic data, several key questions remain unanswered. What spectroscopic or crystallographic evidence supports the assumed stoichiometries and proposed structures of the complexes? Given the fact that most studies date back several decades, combining technological improvements and insights from related systems, some species or structural features can now be verified or falsified. Correspondingly, what are the formation constants associated with the authentic species?

Nuclear magnetic resonance (NMR) is a powerful spectroscopic method for the determination of the structures of organic molecules and their complexes with metal ions. Hence, it has been used for clarifying the structures of some uranyl(VI) malate complexes. These studies revealed that these complexes are predominantly binuclear in nature, with the 2 : 2 uranyl(VI) malate complex being the predominant complex in an equimolar solution at low pH values (pH 2–4). In addition, a uranyl(VI) malate 2 : 1 complex was described, which is also present at low pH values.[35,41,42] There are open questions regarding the structures (including stoichiometry and coordination modes) as well as stability constants of these complexes, which are the subject of the present work. Building upon former investigations, state-of-the-art NMR spectroscopic measurements can provide ^{1}H and ^{13}C NMR spectra with better spectral resolution at much lower concentrations. Modern techniques such as ^{17}O NMR and calculations using density functional theory (DFT) provide deeper insights helping in elucidating possible structures. Determination of thermodynamic parameters including the formation constants ($\log\beta$) is carried out with two different approaches: time-resolved laser-induced fluorescence spectroscopy (TRLFS) and isothermal titration calorimetry (ITC). TRLFS enables the investigation of the species distribution, which can be used for the determination of the complex formation constants. ITC is performed to determine the formation constants and further thermodynamic parameters such as enthalpy (ΔH), entropy (ΔS), and Gibbs energy (ΔG) of the reaction. UV-vis spectroscopy is performed to verify the oxidation state of U and compare it with those of similar systems already studied, for instance uranyl(VI) citrate.

This work aims to gain a deeper understanding of uranyl(VI) complexation with malic acid by addressing both structural and thermodynamic aspects. Structural characterization focuses on dinuclear 2 : 1 and 2 : 2 complexes using NMR spectroscopy and DFT calculations. Thermodynamic data including formation constants and enthalpic/entropic contributions are reinvestigated through TRLFS and ITC. Examination of this specific system has the potential to offer novel insights into the general interactions between uranyl(VI) ions and hydroxycarboxylic acids.

Experimental

Caution! Uranium is an α-emitting radionuclide. The following experiments were performed in a controlled area where the handling of radioactive materials is permitted and regulated.

Sample preparation

All chemicals were used without further purification. For the preparation of uranyl(VI) malate samples, 0.10 M $UO_2(ClO_4)_2$ or 0.010 M $UO_2(NO_3)_2$ stock solutions were used. Stock solutions of malic acid were freshly prepared before each experiment by weighing and dissolving appropriate amounts of L-malic acid (≥99%, Roth) with concentrations ranging from 0 to 20 mM in Milli-Q water (18.2 MΩ cm; Millipore, Merck). To adjust the ionic strength, appropriate aliquots of a 1 M $NaClO_4$ solution ($NaClO_4 \cdot H_2O$, ≥99%, Merck) were added. pH values were adjusted using diluted $HClO_4$ and NaOH solutions using a pH meter (pH720, WTW inolab) equipped with a pH electrode (BlueLine 16 pH electrode, SI Analytics). All samples were prepared at 25 °C.

NMR samples were prepared by the dilution of appropriate aliquots of stock solutions of $UO_2(NO_3)_2$ and malic acid. Because of sample concentrations in the μM range, NMR solutions were prepared in pure D_2O (99.95% D), and pD was adjusted with DCl (99% D) and NaOD (99% D), all purchased from Deutero. pD was corrected for deuterium according to the relationship pD = pH(read) + 0.4.[43]

For TRLFS experiments, uranyl(VI) malate samples were prepared with a U(VI) concentration of 50 μM in 0.1 M $NaClO_4$ solution, where the ligand concentration was varied between 0 and 0.100 M, and adjusted to pH = 4.0. For cryo-TRLFS, the solutions were transferred into plastic cuvettes (Rotilabo disposable UV cuvettes XK26.1, Carl Roth), and then flash-frozen with liquid nitrogen and stored at −80 °C until measurement. TRLFS measurements were performed at −120 °C to avoid quenching effects.

ITC experiments were performed with 30, 50, and 100 μM U(VI) and 1.0 mM malic acid in 0.1 M $NaClO_4$ at pH = 4.0.

UV-vis experiments were performed at pH = 3.0, with concentrations of uranyl nitrate ranging from 50 μM to 5.0 mM, and those of malic acid ranging from 0 through 50 mM, using a 1 mL quartz cuvette.

To prevent any potential light-induced sample degradation, the samples were covered with aluminum foil during their preparation.

Nuclear magnetic resonance spectroscopy (NMR)

NMR spectra were recorded at (25 ± 0.1) °C with an Agilent DD2-600 system operating at 14.1 T with corresponding ^1H, ^{13}C, and ^{17}O resonance frequencies of 599.8, 150.8, and 81.4 MHz using a 5 mm oneNMR™ probe. ^1H NMR spectra were measured by accumulating varying numbers of scans (16 up to over 14 k) depending on the concentrations of the individual sample series, using 2 s of acquisition time and relaxation delay, respectively, applying a 2 s pre-saturation pulse on the water resonance for water signal suppression followed by a π/6 excitation pulse (3.3 μs). ^{13}C data were acquired using broadband ^1H decoupling, 1 s of acquisition time and applying 4 s of relaxation delay after a π/6 (2.9 μs) excitation pulse. Signal assignment was validated by two-dimensional correlation techniques. Therefore, heteronuclear single-quantum coherence (HSQC) and heteronuclear multiple-bond correlation (HMBC) were accomplished using pulse sequences taking advantage of gradient selection and adiabatic pulses. HMBC and HSQC spectra were acquired with 2048 × 1024 complex points in F_2 and F_1, 128 and 96 transitions per F_1 increment, and a relaxation delay of 1 s, respectively. For polarization transfer, $(2J)^{-1}$ delays of 62.5 and 3.57 ms were selected, corresponding to 8 Hz ^nJ in the HMBC and 140 Hz ^1J in the HSQC, respectively. The homonuclear correlation (^1H,^1H-COSY) spectrum of the 10 μM U(VI) solution was acquired with 1 s pre-saturation, 1 s relaxation delay, and 1024 × 128 (F_2 × F_1) complex points and 1024 transitions per F_1 increment. ^1H and ^{13}C NMR spectra were referenced relative to the methyl signal of TMSP-d_4 in D_2O with δ_H and δ_C set to 0.00 ppm. ^{17}O NMR spectra were obtained from direct excitation (23 μs π/2 pulse) without ^1H decoupling, using 100 ms acquisition time and 400 ms relaxation delay. The number of scans varied between 4096 and 360 k, depending on sample composition. The bulk water signal was used as a reference (δ_O = 0 ppm).

Density functional theory (DFT) calculations

Quantum chemical calculations were performed using the Gaussian 16 program (Gaussian Inc.) rev.B01[44] employing DFT by using a conductor-like polarizable continuum model.[45] Structural optimizations were performed at the B3LYP level[46,47] followed by vibrational frequency analysis at the same level to confirm that there was no imaginary frequency present. The energy consistent small-core effective core potential (ECP) and the corresponding basis set suggested by Küchle *et al.* were used for U,[48] whereas correlation consistent cc-pVTZ basis sets were employed on C, O, and H.[49] The most diffuse basis functions on U with the exponent 0.005 (all s-, p-, d-, and f-type functions) were omitted, which made the convergence of the electronic wave function much faster, but had only little effect (less than 1 kJ mol^{-1}) on the total energy. The spin–orbit effects and basis set superposition error corrections were neglected. While spin–orbit effects could be generally important for actinides with partially filled 5f orbitals, it has been confirmed in a previous study that the spin–orbit-coupled uranyl(VI) ground state comprised only the closed-shell ^1A_g state;[50] therefore neglecting spin–orbit effects could be justified, especially when only relative differences in the energy of similar complexes are discussed.

Time-resolved laser-induced fluorescence spectroscopy (TRLFS)

A Nd:YAG laser (Inlite series, Continuum) with frequency quadruplication set at 266 nm was used for luminescence excitation (pulse energy of 3 mJ and pulse width of 5–8 ns) with a pulse repetition rate of 20 Hz. Detection was performed using a spectrometer (iHR 550, slit width: 200 μm, Horiba) equipped with an intensified CCD camera (Horiba) cooled to 4 °C. The spectrometer's central wavelength was calibrated to 546.07 nm using an HG-1 mercury argon calibration lamp (Hg and Ar lines from 253 to 922 nm, Ocean Optics). Spectra were recorded in the wavelength range from 350 to 663 nm with a resolution of 0.1 nm and delay times between 0 and 2500 μs. The spectra were averaged over 50 or 100 accumulations and baseline corrected using LabSpec 5 software (Horiba). For time-resolved measurements, eqn (1) was applied to determine the dynamic step size t_i, which accounts for species with both short and long lifetimes.

$$t_i = 0.1\,\mu s + x\,\mu s \times i + \frac{i^4}{500}\,\mu s \quad (1)$$

where i is the number of steps and x is the minimal step length of 0.005 μs.

All TRLFS data were analysed using parallel factor analysis (PARAFAC) as the N-way toolbox in MATLAB R2020b software (The Mathworks Corporation),[51] as described by Drobot *et al.*[52]

Isothermal titration calorimetry (ITC)

The MicroCal PEAQ-ITC instrument (Malvern Panalytical) was used for ITC. The titration cells have a volume of approximately 200 μL. The titrant (malic acid) was injected into the sample cell using an automated 40 μL syringe at 25.0 °C with continuous stirring at 750 rpm. The titration occurred in 19 steps of 0.5 and 2 μL and a 150 s spacing. The syringe was filled with 1×10^{-3} M malic acid in 0.1 M $NaClO_4$ solution. The sample cell contained 30, 50, and 100 μM U(VI) in a 0.1 M $NaClO_4$ solution at the same pH as that of the malic acid solution. A blank measurement – titration of malic acid to background electrolyte without U(VI) – was performed. The experimental triplicate was analyzed globally in MATLAB R2020b as previously reported.[53] For error estimation, a Monte Carlo approach was used as described elsewhere.[54]

Electronic absorption spectroscopy (UV-vis)

UV-vis spectra were measured using a Varian Cary 5 g spectrophotometer in the spectral range from 700 to 350 nm, using a 10 mm quartz cuvette against ultrapure water in double beam mode. An average time of 100 ms and an interval of 0.25 nm were applied.

Extrapolation to zero ionic strength

For calculating complex formation constants extrapolated to zero ionic strength, the Davies equation was used with the A parameter of 0.5093 $kg^{1/2}$ $mol^{-1/2}$ and the b parameter of 0.3 $kg^{1/2}$ $mol^{-1/2}$.[55]

Results

Determination of the molecular structure

Quantum chemical calculations were performed with a focus on binding motifs, overall molecular structures, and relative Gibbs energies to preselect reasonable species present for the given (experimental) conditions to be included in the thermodynamic model. Calculations focus on dinuclear complexes because these are the only relevant species for the conditions applied.

Fig. 1 depicts calculated structures of 2 : 1 uranyl(VI) malate complexes, all of which are characterized by the presence of a single malate ligand that serves as a bridge between two uranyl(VI) entities. The structure shown in (A) features a bridging hydroxo ligand (μ_2-OH) and a (κ^3O,O′,O″) motif including a bridging alkoxylato group of the malate ligand as proposed by Nunes *et al.*[41] The other species (structures B through E) constitute two uranyl(VI) units being bridged only by malate in various ways. That is, the alkoxyl group coordinates exclusively with one uranyl(VI), while the C1 carboxyl group (structures B–D) or the C4 carboxyl group (structure E) binds concomitantly, resulting in the formation of five- or six-membered ring chelation motifs, respectively. The remaining carboxyl group coordinates the second uranyl(VI) either unidentately (structure D) or bidentately, thereby adjusting the number of water molecules coordinating to the second uranyl(VI) to three (plus one additional explicit second-shell water) or four. The latter configuration yields a hexagonal bipyramid (structures B and C, respectively). Relative to structure B, structures C, D, and E are less stable by +14.5, +7.7, and +18.5 kJ mol^{-1}, respectively.

The structures of the 2 : 2 complex isomers have also been calculated. One isomer possesses a rotational axis perpendicular to the molecular plane while the other isomer possesses a rotational axis perpendicular to the O–U–O axes, corresponding to Fig. 2 structures A and B, respectively. Interestingly, the calculated Gibbs energies reveal that the difference between structures A and B of the 2 : 2 complex is only 1.9 kJ mol^{-1}, slightly favoring the former. Taking into account the inherent uncertainties in the use of density functional theory calculations largely associated with the implicit

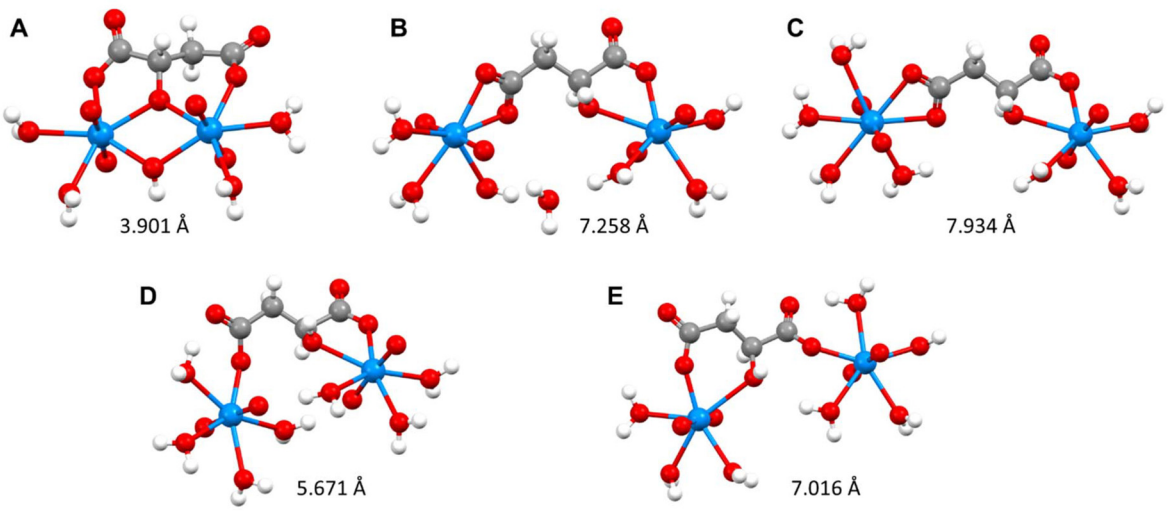

Fig. 1 DFT-calculated structures of species involving two uranyl(VI) units and one malate ligand in different arrangements, along with U–U distances with the structures. Color key: blue, uranium; red, oxygen; grey, carbon; and white, hydrogen. For further details, see the text.

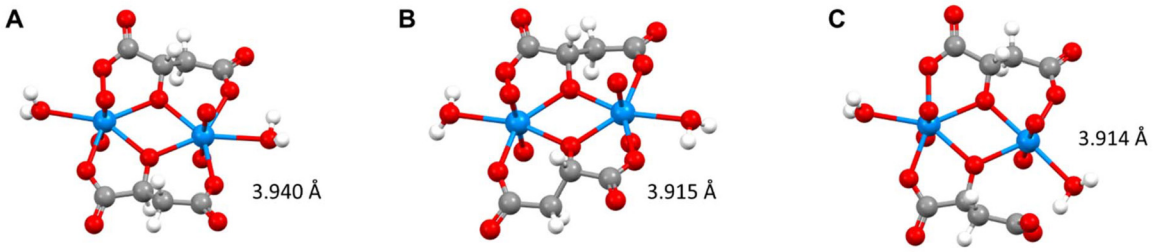

Fig. 2 DFT-calculated structures of species involving two uranyl(VI) units and two malate ligands in different arrangements, along with U–U distances with the structures. Color key: blue, uranium; red, oxygen; grey, carbon; and white, hydrogen. For further details, see the text.

solvation model,[56] this result is in full agreement with the two isomers observable by the NMR experiment in a ratio of ~ 7 : 3 (*cf.* Fig. S1–S5, SI). Just as a rough estimation of the magnitude of the energy contribution from carboxylate binding, the structure given in Fig. 2C reveals a penalty of about 49 kJ mol^{-1} upon dissociation of one uranyl(VI)–carboxyl oxygen bond.

NMR spectroscopy was performed in order to verify the species required to describe the thermodynamic model used in ITC. For the given concentration range and pH (pD) values, the aqueous speciation of U(VI) and malic acid can be described satisfactorily with three uranyl(VI) and three malate species, respectively: the free uranyl(VI) aquo ion and the free ligand as well as the two dinuclear complexes with 2 : 1 and 2 : 2 U(VI) : malate ratios, the latter of which is present as two geometric isomers[35,41,42] that are invariant in their molar ratio (throughout 70 : 30). NMR spectra associated with the 2 : 1 and 2 : 2 complexes are depicted in Fig. 3 and 4.

This set of spectra was recorded to unambiguously identify the species upon comparison with and to complement literature data by means of ^{17}O NMR spectra. Since the 2 : 1 complex is of C_1 symmetry, all sites are unique. Due to the complex's inherent asymmetry arising from the chirality of the ligand, the two uranyl(VI) entities exhibit distinct characteristics. That is, one uranyl(VI) unit is a part of a five-membered

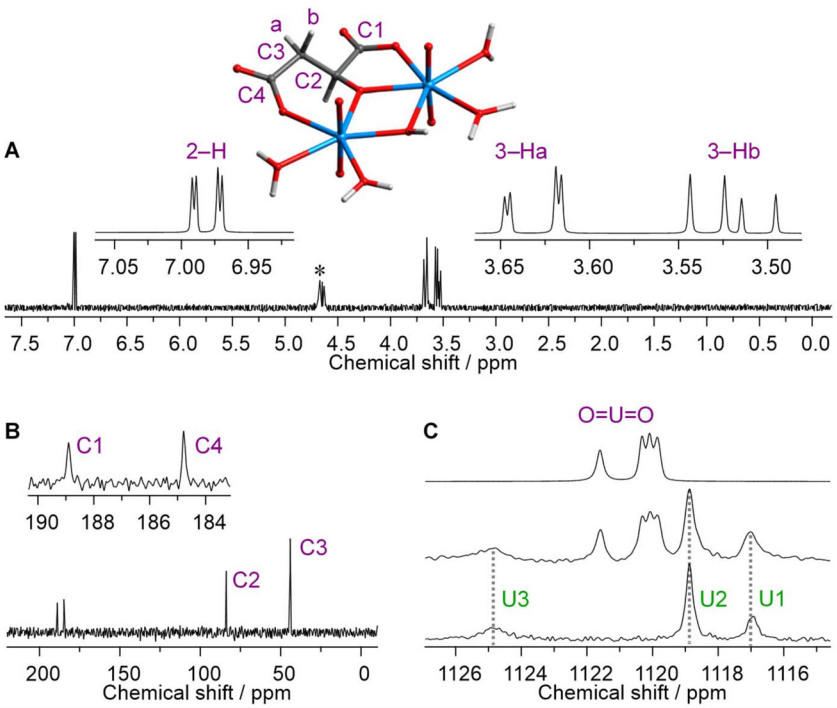

Fig. 3 Uranyl(VI) malate 2 : 1 complex: (A) ^{1}H NMR spectrum showing the three 2 : 1 complex-associated signals of the CH group (C2) as well as that of the CH_2 group (C3) possessing diastereotopic hydrogens with distinct resonances (*a*/*b*). The asterisk indicates the residual signal from solvent (HDO) signal suppression. (B) ^{13}C{^{1}H} NMR spectrum showing the four 2 : 1 complex-associated signals of the two carboxyl (C1 and C4) carbons as well as of the CH group (C2) and of the CH_2 group (C3). (C) ^{17}O NMR of UO_2 oxygen atoms. The bottom spectrum is a reference spectrum showing signals of three aqueous uranyl(VI) species (U1–U3) with different degrees of hydrolysis; [U(VI)] = 58 mM, pD 3.5. U1, U2, and U3 refer to the UO_2^{2+} aquo ion, the dinuclear $(UO_2)_2(OH)_2^{2+}$ and the trinuclear $(UO_2)_3(O)(OH)_3^{+}$ species, respectively.[57] The middle spectrum was obtained from a D_2O solution with [U(VI)] = 58 mM, [malate] = 17 mM, pD 3.5, with the corresponding four 2 : 1 complex-associated signals extracted from deconvolution shown as the top spectrum. Signal assignment in NMR spectra is according to the labeling stated with the structure.

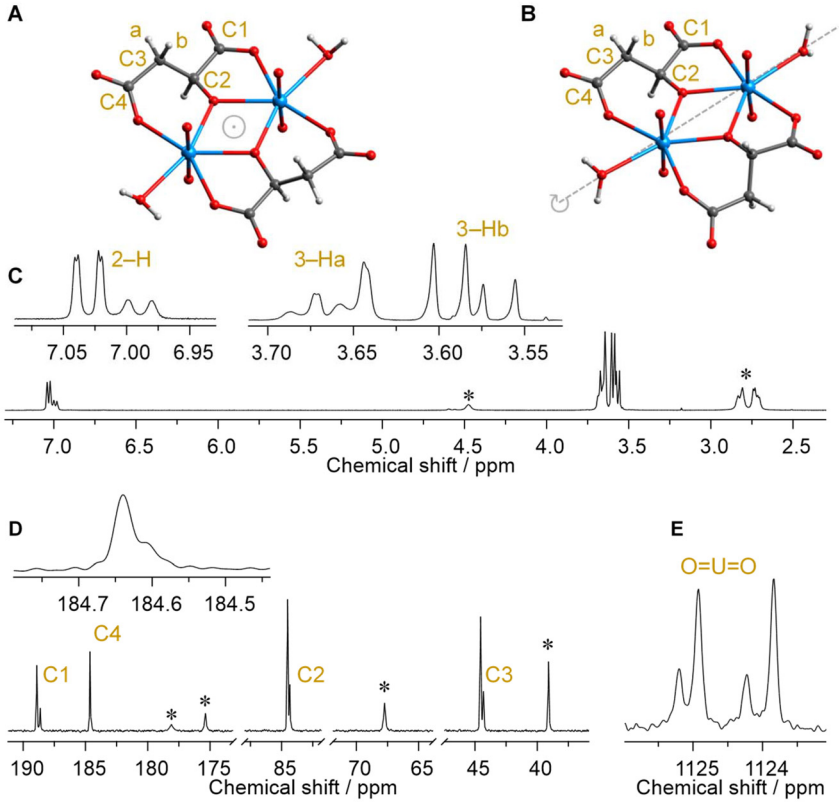

Fig. 4 Uranyl(VI) malate 2 : 2 complex isomers: both isomers feature C_2 symmetry, with the C_2 rotational axes being perpendicular to the molecular plane (A) and perpendicular to the O–U–O axes (B), respectively. Signal assignment in NMR spectra is according to the labeling with the structures. All NMR spectra (C, D, and E) show two sets of signals each associated with one of the 2 : 2 complex's isomers, *i.e.*, one set of intense signals referring to the main isomer and one set of less intense signals referring to the minor isomer. Asterisks denote signals due to the excess ligand. (C) ^{1}H NMR spectrum showing the 2 : 2 complex-associated signals of the CH group (C2) as well as of the CH_2 group (C3) possessing diastereotopic hydrogens with distinct resonances (a/b). (D) ^{13}C NMR spectrum showing the four 2 : 2 complex-associated signals of the two carboxyl (C1 and C4) carbons as well as those of the CH group (C2) and the CH_2 group (C3). (E) ^{17}O NMR spectrum of UO_2 oxygen atoms. The spectra were obtained from a D_2O solution with [U(VI)] = 250 mM, [malate] = 500 mM, pD 3.5.

ring chelation motif while the other features a six-membered ring. Consequently, the two uranyl(VI) units, each bearing two "yl"-oxygens, give rise to four distinct signals (Fig. 3C).

In the case of the 2 : 2 complex, both isomers feature C_2 symmetry, with the C_2 rotational axes being perpendicular to the molecular plane or perpendicular to the O═U═O axes (Fig. 4), respectively. Correspondingly, in one isomer, each uranyl(VI) is part of a five- and a six-membered ring chelation motif. In the other isomer, one uranyl(VI) is part of two five-membered ring chelation motifs while the other uranyl(VI) is part of two six-membered ring chelation motifs, *cf.* Fig. 4A and B, respectively. Within one 2 : 2 complex isomer species, the two ligands involved are equivalent by symmetry. However, owing to the difference in overall symmetry the isomers behave as diastereomers, giving rise to individual sets of signals. Therefore, the NMR spectra show two sets of signals: one set of intense signals referring to the main isomer and one set of less intense signals referring to the minor isomer.

In principle, the ligand gives rise to three ^{1}H and four ^{13}C signals. Since the methylene protons are diastereotopic, they show distinct resonances, at δ_H around 2.7 and 2.8 ppm as well as between 3.5 and 3.7 ppm for the free and U(VI) bound ligand, respectively. Owing to the scalar spin–spin coupling between each other (*geminal* coupling, $^{2}J_{H,H}$) and to the adjacent CH (*vicinal* coupling, $^{3}J_{H,H}$), each signal appears as a more or less resolved doublet of doublets, showing signal splitting with a characteristic coupling constant (Karplus relationship). Upon complexation, the ^{1}H signals shift downfield, especially that of the CH group is displaced by about 2.5 ppm (*cf.* Fig. S1, SI), which can be mainly attributed to the electron withdrawing effect of two uranyl(VI) entities (each with an effective charge of +3.2)[58] being bridged (μ_2-O) by the adjacent hydroxylate group.

Because of the reduced number of potentially overlapping lines, and the sensitivity of ^{1}H NMR spectroscopy, the CH groups' ^{1}H signals are well-suited for the discrimination between species (Fig. S1, SI, black rectangle).

The ^{1}H NMR spectra of the pD-titration series with concentrations analogous to those in ITC experiments, obtained at varying U(VI) to malate ratios, as well as those of the additional pD- and concentration-dependent series, are provided as Fig. S2 and S6, SI. All these spectra taken together reveal the

ranges of existence of the species of interest from the ligand's perspective.

Although the CH signals of the 2 : 1 complex and the 2 : 2 complex's minor isomer are very close, *viz.* δ_H 6.99 and 6.98 ppm, respectively, taking into account that the most downfield signal (δ_H 7.03 ppm) refers to the major isomer, and both isomers' signals appear invariantly in a 7 : 3 intensity ratio, the spectral signature of all three complex species allows for reliable qualitative and quantitative assignment. Considering that in the 2 : 1 and 2 : 2 uranyl(VI) malate complexes one and two ligand molecules contribute to the resulting signals, for excess U(VI), the relative fractions of the 2 : 1 *vs.* 2 : 2 species (both isomers) are 0.66 *vs.* 0.34 at pD 3.0 and 0.91 *vs.* 0.09 at pD 5.0, respectively (Fig. S2A, SI). In the case of equimolar (100 μM) U(VI) and malic acid, the relative fractions (2 : 1 *vs.* 2 : 2 species) change from 0.56 *vs.* 0.44 at pD 3.0 to 0.82 *vs.* 0.18 at pD 5.0 (Fig. S2B, SI). For 10 μM U(VI) and tenfold ligand excess, at pD 5 the corresponding relative fractions amount to 0.07 *vs.* 0.93 (Fig. S2C, SI). Signal intensities in the pD 2.0 spectrum are too low for quantification. Notably, within the detection limits of NMR, regardless of composition, U(VI) complexation starts at pD 3.0, and even for U(VI) concentrations as low as 10 μM, the observed complex species are dinuclear. In the range 3.0 < pH/pD < 5.6 and ligand excess, the 2 : 2 species are predominant. Supplementary results are obtained by UV-vis spectrophotometry and are consistent among the other methods. Corresponding spectra are provided in Fig. S10 and S11, SI. Briefly, both the wavelength at the absorption maximum $\lambda(\varepsilon_{max})$ and the maximum molar absorptivity ε_{max} of the uranyl(VI) chromophore increase upon addition of malic acid, however, with significant differences for the given U(VI) to malate ratios. That is, spectral characteristics change from 9.3 M^{-1} cm^{-1} at 414 nm (uranyl(VI) nitrate pH 3 solution) to 30.4 M^{-1} cm^{-1} at 427 nm for the 2 : 1 uranyl(VI) malate complexes and to 80.5 M^{-1} cm^{-1} at 434 nm for the 2 : 2 uranyl(VI) malate complexes, respectively.

Thermodynamics of the uranyl(VI) malate complexes

NMR and DFT presented two distinct main complexes from the interaction of uranyl(VI) and malic acid according to different molar ratios of the compounds. The complexes were identified as 2 : 1 and 2 : 2 uranyl(VI) malate complexes. After the verification of the stoichiometry and structures of these complexes, complex formation constants and thermodynamic parameters of these complexes were determined using TRLFS and ITC series.

For the calculation of the thermodynamic parameters, eqn (2) and (3) were considered as the equilibrium reactions for the 2 : 1 and 2 : 2 complexes, respectively. These formulas take into account the deprotonation of the carboxylic groups and also of the hydroxyl group (Mal_{-H}^{3-}) as an essential part of the dinuclear structures of the 2 : 1 and 2 : 2 uranyl(VI) malate complexes.

$$2UO_2^{2+} + Mal_{-H}^{3-} + OH^- \rightleftharpoons (UO_2)_2(OH)(Mal_{-H})^0(aq) \quad (2)$$

$$2UO_2^{2+} + 2Mal_{-H}^{3-} \rightleftharpoons (UO_2)_2(Mal_{-H})_2^{2-} \quad (3)$$

Time-resolved laser-induced luminescence spectroscopy

Uranyl(VI) malate samples were prepared at pH 4, each containing a fixed U(VI) concentration of 50 μM and varying concentrations of malate (0–109 μM), followed by rapid freezing in liquid nitrogen. An additional sample containing 10 mM malate was prepared to assess the effect of a substantial ligand excess on U(VI) speciation.

All samples were analyzed under identical experimental conditions, thereby fulfilling the trilinearity condition required for PARAFAC. The fluorescence data were evaluated using the N-Way Toolbox in MATLAB R2020b. Speciation was constrained to the previously identified uranyl(VI) malate complexes, as described elsewhere.[59] The resulting emission spectra and species distributions are presented in Fig. 5, while the spectral features of the individual species are summarized in Table 1.

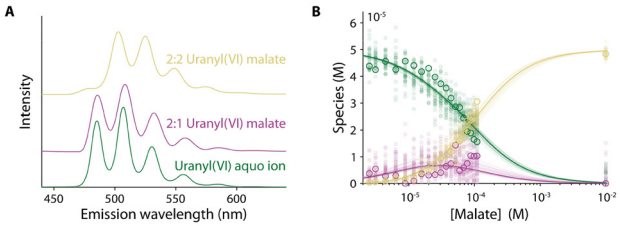

Fig. 5 PARAFAC results extracted from TRLFS data of the complexation of malic acid with U(VI) at pH 4. [U(VI)] = 50 μM, [malate] = 0–10 mM, [$NaClO_4$] = 0.1 M. (A) Individual spectra of U(VI) species in solution. (B) Quantum yield-corrected PARAFAC species distribution as a function of the malate concentration. Color code: green, uranyl(VI) aquo ion; magenta, 2 : 1 uranyl(VI) malate complex; and yellow, 2 : 2 uranyl(VI) malate complex.

Table 1 Emission spectral peak positions expressed in nm of the three different U(VI) species as obtained from TRFLS series. Data in parentheses represent peaks of low intensity

Species	Luminescence emission bands (nm)				
Uranyl(VI) cation	485	507	530	556	(584)
2 : 1 uranyl(VI) malate	486	508	532	558	(586)
2 : 2 uranyl(VI) malate	(476)	503	525	549	(574)

This targeted speciation enabled the extraction of formation constants for the uranyl(VI) malate complexes. Based on reactions (2) and (3), we determined log β values of 16.7 ± 0.1 for the 2 : 1 complex and 37.6 ± 0.1 for the 2 : 2 complex. Additional information regarding the TRLFS data is provided as Fig. S8, SI.

Isothermal titration calorimetry

To validate the thermodynamic parameters derived from TRLFS, ITC was employed as an independent and complementary technique. Unlike TRLFS, which probes electronic transitions of uranyl(VI) complexes, ITC directly measures the heat exchanged during complexation reactions, providing insight into the underlying enthalpic and entropic contributions.

Malic acid (1 mM) was titrated into aqueous U(VI) solutions at pH 4 in 19 individual injections, using three different U con-

centrations (30 μM, 50 μM, and 100 μM). These variations were chosen to simultaneously ensure reproducibility and moderate shifts of the concentration windows explored. Background heat effects were corrected by subtracting a blank titration (malate into buffer without U(VI)). The ITC data were analyzed using the same speciation model as applied for the TRLFS data evaluation.

Fig. 6 illustrates representative results for the 100 μM U(VI) titration, including the raw thermogram (A), the integrated heat curve and model fit (B), and the calculated species distribution (C). The corresponding results for the other U(VI) concentrations (30 and 50 μM) are provided as Fig. S9, SI.

The extracted formation constants were $\log\beta = 17.1 \pm 0.1$ for the 2 : 1 uranyl(VI) malate complex and $\log\beta = 37.7 \pm 0.1$ for the 2 : 2 uranyl(VI) malate complex. Consistent with previous studies on the complexation of f-block elements with aminocarboxylates,[17] both complexation reactions were endothermic, indicating entropy-driven processes. The entropy contributions are likely attributed to stripping of coordinated water molecules from both the metal ion and the ligand during complex formation. Gibbs free energies (ΔG) and entropy changes (ΔS) were calculated using eqn (4) and (5):

$$\Delta G = -RT \ln (K) \quad (4)$$

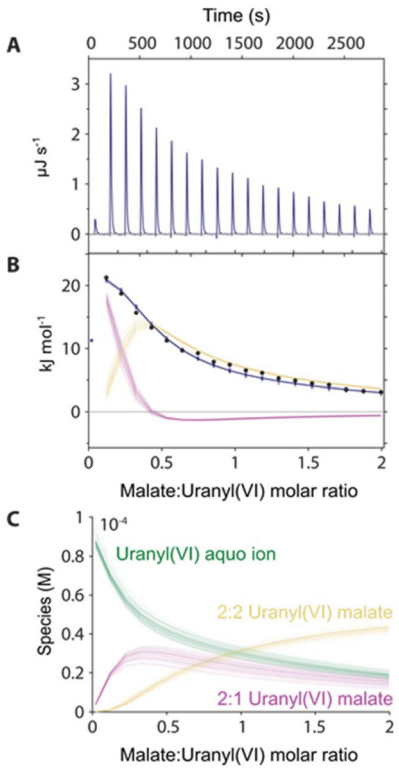

Fig. 6 ITC results of the complexation of malic acid with U(VI) at pH 4. $[U(VI)]_{initial}$ = 100 μM, [malate] = 0–220 μM, $[NaClO_4]$ = 0.1 M. (A) Thermogram obtained from the ligand to metal titration. (B) Integrated heat and best fit (blue line). (C) Derived distribution of the U(VI) species involved. Color code: green, uranyl(VI) aquo ion; magenta, 2 : 1 uranyl(VI) malate complex; and yellow, 2 : 2 uranyl(VI) malate complex.

$$\Delta G = \Delta H - T\Delta S \quad (5)$$

A summary of all thermodynamic parameters obtained is provided in Table 2.

Table 2 Thermodynamic parameters obtained from ITC for the 2 : 1 and 2 : 2 uranyl(VI) malate complexes at 25 °C in 0.1 M $NaClO_4$ aqueous solution

Complex species	$\log\beta$ [a] (ITC)	ΔH (kJ mol^{-1})	ΔG (kJ mol^{-1})	ΔS (kJ mol^{-1} K^{-1})
2 : 1 uranyl(VI) malate	17.1 ± 0.1	11.0 ± 0.1	−97.9	0.365
2 : 2 uranyl(VI) malate	37.7 ± 0.1	27.5 ± 0.8	−215.1	0.814

[a] I = 0.1 M $NaClO_4$.

Complex formation constants ($\log\beta$)

Table 3 summarizes the formation constants obtained from TRLFS and ITC. To ensure comparability with literature data, the experimentally determined $\log\beta$ values were extrapolated to standard conditions (zero ionic strength, I = 0 M) using the Davis model.[55] The complex formation constants from ITC are in very good agreement with those obtained using TRLFS. This agreement highlights the reliability of these $\log\beta$ values from different independent experiments with same conditions (molar ratios, pH, and ionic strength).

Table 3 Formation constants of 2 : 1 and 2 : 2 uranyl(VI) malate complexes at 25 °C. Uncertainties are represented by the standard deviation of at least three independent experiments

Complex species	$\log\beta$ [a] (TRLFS)	$\log\beta^0$ [b] (TRLFS)	$\log\beta$ [a] (ITC)	$\log\beta^0$ [b] (ITC)
2 : 1 uranyl(VI) malate	16.7 ± 0.1	17.1 ± 0.1	17.1 ± 0.1	17.5 ± 0.1
2 : 2 uranyl(VI) malate	37.6 ± 0.1	37.4 ± 0.4	37.7 ± 0.1	37.5 ± 0.4

[a] I = 0.1 M $NaClO_4$. [b] Extrapolated to zero ionic strength using Davies equation with the following parameters: A = 0.5093 kg$^{1/2}$ mol$^{-1/2}$ and b = 0.3 kg$^{1/2}$ mol$^{-1/2}$.[55]

Discussion

The distance between the uranium atoms, d(U–U), is a very valuable feature experimentally determined by EXAFS measurements[38,60] which can be compared to those in DFT-calculated structures (Fig. 1 and 2). EXAFS results from Allen *et al.*,[38] who did not state the malic acid used (which enantiomer or racemic mixture), characterize the uranyl(VI) malate dimeric complex by a d(U–U) of about 3.93 Å. The d(U–U) values in the DFT-calculated structures, 3.901 Å for the 2 : 1 complex as well as 3.940 and 3.915 Å for the two 2 : 2 complex isomers, are in excellent agreement with the experimental value, evidencing the proximity of the two uranyl(VI) entities caused by the (κ^3O,O′,O″) motif including a bridging alkoxylato group of the malate ligand for both complexes and ruling out structures B through E in Fig. 1.

The uranyl(VI) 2 : 2 complexes of both malate and citrate are isostructural and reveal very much similar spectroscopic features.[16] That is, the ε_{max} at $\lambda(\varepsilon_{max})$ is 80.5 M^{-1} cm^{-1} at 434 nm in the case of malate and 83 M^{-1} cm^{-1} at 435 nm in the case of citrate.[61] In both cases, d(U–U) is determined as (3.93 ± 0.02) Å,[38] and the uranyl(VI) oxygens give rise to distinct ^{17}O NMR signals mirroring the involvement of two ligands and two uranyl(VI) entities.[16] With reference to the citrate system, taking into account the alkoxyl group's pK_a value of 14.5,[15] the complex stability of the corresponding citrate complex amounts to a log β of 34.2 ± 0.1 (in 0.1 M $NaClO_4$) and thus is similar to the 37.6 ± 0.1 determined for the uranyl(VI) malate 2 : 2 complex. Both these stability constants are very large in their own right, and yet that of the malate complex is still 3 logarithmic units larger. Besides slightly more basic carboxyl groups and less steric demands in malate, we hypothesize that the kinetic effects in the citrate complexes are responsible for the weakening. That is, citrate's additional $CH_2COO(H)$ residue, by means of NMR line widths and exchange spectroscopy shown to be involved in intramolecular site exchange reactions,[16] slightly reduces the overall stability. In contrast, the malate complexes lack such a feature since all of the ligand functional groups are involved in coordination.

Interestingly, the 2 : 1 complex not only contains the malate ligand bridging between two uranyl(VI) entities but also a bridging μ-OH ligand. In both the 2 : 1 and 2 : 2 complexes, the bridging of of two uranyl units by malate's hydroxyl group is the consequence of metal ion-promoted H^+ abstraction. The same phenomenon is observed for coordinating water ligands being deprotonated at a pH far below the corresponding pK_a (*i.e.* hydrolysis). Since under the given conditions (50 μM U(VI), pH 4) the presence of other hydroxo species such as $UO_2(OH)^+$ or $(UO_2)_2(OH)_2^{2+}$ is negligible,[62] one can speculate that in the first instance the bridging malate complexation eases the concomitant approaching of the two uranyl(VI) units. The latter subsequently facilitates proton abstraction from coordinating water yielding the bridging hydroxo ligand resulting in the $[(UO_2)_2(\mu_2\text{-OH})(Mal_{-H})]^0(aq)$ complex (for the given U excess). This pathway can be sketched as the (fast/complete) transition from structure D to structure A in Fig. 1.

Feldman and Havill studied U(VI) and malate complexation in acidic solutions with a 10 mM U(VI) concentration. They found two distinct complexes with U/malate stoichiometric ratios of 1 and 2, respectively. The former species was predominant under equimolar and ligand excess conditions up to pH 4.8.[39] In our work at pH 3.5, no complex with a U/malate stoichiometric ratio <1 (such as a 1 : 2 uranyl(VI) malate complex) was detected. Hence, under the conditions investigated, three distinct U(VI) species are observed, *viz.* uranyl(VI) aquo ions as well as 2 : 1 and 2 : 2 uranyl(VI) malate complexes. In a subsequent study at pH 3.5–11, Feldman *et al.*[63] addressed the binding motifs and complex structures, concluding that tridentate ligand binding already occurred in acidic solution. Assuming that each ligand coordinates only one uranyl(VI) at a time and that alkoxyl groups do not deprotonate in acidic solution, they struggled to bring in accordance the complexes' structures and the number of titrated H^+, requiring the inclusion of two bridging hydroxide ions (μ_2-OH) in their proposed structure. In a later study, Feldman *et al.*[34] stated that within the pH range of 2–4, the speciation is dominated by binuclear tridentate complexes of 1 : 1 stoichiometry, with the proposed structure later proven to be correct.

From potentiometric titrations in the pH range 2–8, Rajan and Martell[36] concluded that, in accordance with earlier studies, at pH 2–4 the complexes are binuclear, bridged by ligand functional groups. They erroneously assumed that the binuclear complex forms in a straight and simple reaction through dimerization of two mononuclear 1 : 1 complexes. It was hypothesized that, in the mononuclear complex, malate would act as a tridentate ligand, while the alkoxyl group would undergo deprotonation. This has resulted in an inaccurate depiction of the equilibrium thermodynamics and the associated equations. This inaccuracy arises from the consideration of the pK_a values of the carboxyl groups, while the pK_a value of the ligand's OH group is overlooked. Therefore, the reported stability constants are of little use.

A further study reported on potentiometric and calorimetric titrations performed at 1–10 mM U(VI), presumably at low pH (not stated).[40] Although stating that 5-membered rings are the most stable binding motif, without any evidence of the complex structure but just by analogy for the sake of comparing ligands of the same carbon chain length, malate is depicted to coordinate (solely) by its two carboxyl groups, thereby forming a 7-membered ring. The determined log K values are assigned to uranyl(VI) malate complexes of 1 : 1 and 1 : 2 stoichiometry. However, from our own observations along with those discussed above with binuclear complexes that are predominant, we consider the assignment and the accompanied stability constants questionable.

In principle, we do not dispute the existence of mononuclear 1 : 1 and/or 1 : 2 uranyl(VI) malate complexes. Given the numerous studies at low pH (and rather high concentrations), for uranyl(VI) complexation not only by malate but also by its related compounds tartrate and citrate, repeatedly evidencing the superior formation of binuclear complexes, we believe that mononuclear complexes have a narrow range of existence. That is, they exist in relevant (detectable) quantities only at sufficiently low pH or/and in very dilute solutions, both conditions preventing bridging between two uranyl(VI) entities. As dilution beyond the micromolar range hampers spectroscopic detectability, we acquired the NMR spectra of D_2O solutions 10 mM in U(VI) and 250 mM in malate at pD 1.5 through 3.0 as well as a pD 3.5 spectrum for 10 μM U(VI) and 100 μM malate (Fig. S6 and S7, SI). The mononuclear complexes constitute coordination by the CH(OH)COOH moiety, *i.e.*, a 5-membered ring chelation motif by the more acidic carboxyl group and the protonated alkoxyl group, leaving the CH_2COOH residue unbound. This is inferred from the downfield shift of the CH(OH) ^1H signal to ~5.3 ppm (compared to the 4.6 ppm in the free ligand at a comparable pD but the ~7.1 ppm of the dinuclear complexes), while the unbound CH_2COOH is merely shifted (*cf.* Fig. S7, SI). The spectra indicate that the mono-

nuclear species are (a) predominant only at the lowest pD values, (b) occur as two complexes, attributed to 1 : 1 and 1 : 2 uranyl(VI) malates, and (c) show an upfield shift of the ^{1}H signals (best seen for CH(OH)) ascribed to the (commencing) deprotonation of the less acidic CH_2COOH carboxyl group, corroborating that this residue is unbound. Due to the very small existence range, and limited accessibility with analytic methods caused by the overall low concentration, we consider the determination of trustworthy thermodynamic quantities (above all, stability constants) of mononuclear uranyl(VI) malate species truly challenging. Nonetheless, our observations underscore the dominance and relevance of binuclear species, already at U(VI) concentrations as low as 10^{-5} M.

Conclusions

Consistent among NMR, TRLFS, ITC, and UV-vis data, the prevalence and species distribution of uranyl(VI) malate complexes are significantly dependent on the molar ratio of U(VI) and malate. For $3 \leq pH \leq 5$, besides the uranyl(VI) aquo ion, the 2 : 1 complex is the predominant uranyl(VI) malate species as long as U(VI) is in excess, otherwise, *i.e.*, for equimolar or malate excess conditions, both the free uranyl(VI) aquo ion and the 2 : 1 complex are displaced by the 2 : 2 uranyl(VI) malate complex. Even in the micromolar concentration range, complex species detected by TRLFS and NMR were essentially dinuclear.

Comprehensive NMR spectroscopic measurements were performed to study the structures and stoichiometry of the complexes in solution under various conditions to support the TRLFS and ITC data interpretation. The results show that the 2 : 2 uranyl(VI) malate complex is predominant over a broad pH range from 3 to 6 even at concentrations as low as 10 μM. The 2 : 1 uranyl(VI) malate was also detected, but at lower pH values (2–4). DFT calculations assisted in the interpretation of NMR spectra and helped to unambiguously assign the individual species. Thermodynamic data were determined by TRLFS and ITC. New binding affinities and stability constants for both complexes (2 : 2 and 2 : 1 complexes) in 0.1 M $NaClO_4$ solutions were determined.

The assignment of the two 2 : 2 complex isomers to the obtained individual sets of NMR signals is not a trivial task and requires further systematic investigation, which is beyond the scope of this study but might be a subject of future work.

The present results enhance our knowledge of U(VI) interaction with malic acid, and significantly improve both the structural elucidation and the thermodynamic database for modeling radionuclide behavior in the biogeosphere. Essential for radioecological aspects, the data contribute to a more reliable prediction of the bioavailability and mobility of radionuclides in the environment in general and in the rhizosphere in particular, which can ultimately contribute to more reliable safety and risk assessments for humans and environment as well as help in refining remediation strategies.

Author contributions

R. E. L.-J.: investigation and writing – original draft; B. D.: conceptualization, methodology, formal analysis, software, visualization, and writing – review & editing; R. S.: formal analysis, visualization, and writing – review & editing; S. T.: investigation, formal analysis, visualization, and writing – review & editing; D. G.: investigation; T. S.: supervision and writing – review & editing; S. S.: conceptualization, project administration, supervision, and writing – review & editing; J. K.: conceptualization, investigation, formal analysis, visualization, writing – original draft, and writing – review & editing.

Conflicts of interest

There are no conflicts to declare.

Data availability

The original contributions presented in this study are included in the article and its supplementary information (SI). Additional spectroscopic and calorimetric results are provided as supplementary material. Figures S1–S7, concentration- and pH-dependent ^{1}H NMR spectra (down to the micromolar concentration range). Figure S8: PARAFAC results of three independent TRLFS series of uranyl(VI) complexation at different malate concentrations. Figure S9, ITC titrations of malic acid with different U(VI) concentrations. Figures S10–S11, UV-vis absorption spectra (and corresponding single-component spectra) obtained from pH 3 solutions of varying uranyl(VI) nitrate and malic acid concentrations. See DOI: https://doi.org/10.1039/d5dt02117k.

Further inquiries can be directed to the corresponding author.

Acknowledgements

This study is a part of the TRAVARIS project, which is funded by the German Federal Ministry of Research, Technology and Space (BMFTR) under contract No. 15S9437C. We thank Frank Bok for valuable discussions about thermodynamic parameters and Sabrina Beutner for ICP-MS measurements.

References

1 I. Goldberg and J. S. Rokem, *Encycl. Microbiol.*, 2009, 421–442.
2 E. Delhaize, S. Craig, C. D. Beaton, R. J. Bennet, V. C. Jagadish and P. J. Randall, *Plant Physiol.*, 1993, **103**, 685–693.
3 L. R. M. de Andrade, M. Ikeda, L. I. V. do Amaral and J. Ishizuka, *Plant Physiol. Biochem.*, 2011, **49**, 55–60.
4 B. Morra and A. A. Olsen, *Chem. Geol.*, 2020, **558**, 119887.

5 E. Hoffland, R. van den Boogaard, J. Nelemans and G. Findenegg, *New Phytol.*, 1992, **122**, 675–680.
6 O. Wiche, C. Dittrich, O. Pourret, N. Monei, J. Heim and H. Lambers, *Plant Soil*, 2023, **489**, 645–666.
7 J. Jessat, H. Moll, W. A. John, M.-L. Bilke, R. Hübner, J. Kretzschmar, R. Steudtner, B. Drobot, T. Stumpf and S. Sachs, *J. Hazard. Mater.*, 2022, **439**, 129520.
8 T. Rudrappa, K. J. Czymmek, P. W. Paré and H. P. Bais, *Plant Physiol.*, 2008, **148**, 1547–1556.
9 V. Lakshmanan, S. L. Kitto, J. L. Caplan, Y.-H. Hsueh, D. B. Kearns, Y.-S. Wu and H. P. Bais, *Plant Physiol.*, 2012, **160**, 1642–1661.
10 Y. Chen, S. Cao, Y. Chai, J. Clardy, R. Kolter, J. h. Guo and R. Losick, *Mol. Microbiol.*, 2012, **85**, 418–430.
11 S. de Weert, H. Vermeiren, I. H. Mulders, I. Kuiper, N. Hendrickx, G. V. Bloemberg, J. Vanderleyden, R. De Mot and B. J. Lugtenberg, *Mol. Plant-Microbe Interact.*, 2002, **15**, 1173–1180.
12 J. A. Lee, J. H. Ahn and S. Y. Lee, in *Comprehensive Biotechnology*, ed. M. Moo-Young, Pergamon, Oxford, 3rd edn, 2019, pp. 172–187.
13 R. M. Zelle, E. De Hulster, W. A. Van Winden, P. De Waard, C. Dijkema, A. A. Winkler, J.-M. A. Geertman, J. P. Van Dijken, J. T. Pronk and A. J. Van Maris, *Appl. Environ. Microbiol.*, 2008, **74**, 2766–2777.
14 R. G. Butz and R. C. Long, *Plant Physiol.*, 1979, **64**, 684–689.
15 A. M. N. Silva, X. Kong and R. C. Hider, *BioMetals*, 2009, **22**, 771–778.
16 J. Kretzschmar, S. Tsushima, C. Lucks, E. Jäckel, R. Meyer, R. Steudtner, K. Müller, A. Rossberg, K. Schmeide and V. Brendler, *Inorg. Chem.*, 2021, **60**, 7998–8010.
17 S. Friedrich, C. Sieber, B. Drobot, S. Tsushima, A. Barkleit, K. Schmeide, T. Stumpf and J. Kretzschmar, *Molecules*, 2023, **28**, 4881.
18 S. Zenker, J. Lohmann, I. Chiorescu, S. Krüger, M. U. Kumke, T. Reich, K. Schmeide and J. Kretzschmar, *Inorg. Chem.*, 2025, **64**(16), 7970–7987.
19 B. Flem, C. Reimann, K. Fabian, M. Birke, P. Filzmoser and D. Banks, *Appl. Geochem.*, 2018, **88**, 133–148.
20 S. Sachs, G. Geipel, F. Bok, J. Oertel and K. Fahmy, *Environ. Sci. Technol.*, 2017, **51**, 10843–10849.
21 M. Carriere, L. Avoscan, R. Collins, F. Carrot, H. Khodja, E. Ansoborlo and B. Gouget, *Chem. Res. Toxicol.*, 2004, **17**, 446–452.
22 N. Gao, Z. Huang, H. Liu, J. Hou and X. Liu, *Chemosphere*, 2019, **237**, 124548.
23 B. Panda, B. Basu, C. Acharya, H. Rajaram and S. K. Apte, *Aquat. Toxicol.*, 2017, **182**, 205–213.
24 S. Akash, B. Sivaprakash, V. C. V. Raja, N. Rajamohan and G. Muthusamy, *Environ. Pollut.*, 2022, **302**, 119068.
25 B. Vellingiri, *Environ. Res.*, 2023, **233**, 116430.
26 M. Ma, R. Wang, L. Xu, M. Xu and S. Liu, *Environ. Int.*, 2020, **145**, 106107.
27 E. S. Craft, A. W. Abu-Qare, M. M. Flaherty, M. C. Garofolo, H. L. Rincavage and M. B. Abou-Donia, *J. Toxicol. Environ. Health, Part B*, 2004, **7**, 297–317.
28 Z. Li, P. Sun, C. Zhang, N. Zhu, N. Xu, D. Li, Y. Gao and J. Zhao, *J. Hazard. Mater.*, 2024, **478**, 135499.
29 M. Anke, O. Seeber, R. Müller, U. Schäfer and J. Zerull, *Geochemistry*, 2009, **69**, 75–90.
30 H. G. Brittain, *Profiles Drug Subst., Excipients, Relat. Methodol.*, 2001, **28**, 153–195.
31 A. Deepatana, J. A. Tang and M. Valix, *Miner. Eng.*, 2006, **19**, 1280–1289.
32 N. Chumha, S. Kittiwachana, T. Thongtem, S. Thongtem and S. Kaowphong, *Mater. Lett.*, 2014, **136**, 18–21.
33 A. Kocaman, *Plant Signaling Behav.*, 2023, **18**, 2064072.
34 I. Feldman, C. A. North and H. B. Hunter, *J. Phys. Chem.*, 1960, **64**, 1224–1230.
35 J. D. Pedrosa and V. M. Gil, *J. Inorg. Nucl. Chem.*, 1974, **36**, 1803–1807.
36 K. Rajan and A. Martell, *J. Inorg. Nucl. Chem.*, 1964, **26**, 1927–1944.
37 E. Cole, E. Flores, M. Basile, A. Jayasinghe, J. De Groot, D. K. Unruh and T. Z. Forbes, *Polyhedron*, 2016, **114**, 378–384.
38 P. G. Allen, D. K. Shuh, J. J. Bucher, N. M. Edelstein, T. Reich, M. A. Denecke and H. Nitsche, *Inorg. Chem.*, 1996, **35**, 784–787.
39 I. Feldman and J. R. Havill, *J. Am. Chem. Soc.*, 1954, **76**, 2114–2117.
40 A. Kirishima, Y. Onishi, N. Sato and O. Tochiyama, *Radiochim. Acta*, 2008, **96**, 581–589.
41 M. T. Nunes, V. M. Gil and A. V. Xavier, *Can. J. Chem.*, 1982, **60**, 1007–1018.
42 M. T. Nunes and V. M. Gil, *Inorg. Chim. Acta*, 1990, **170**, 59–63.
43 P. K. Glasoe and F. Long, *J. Phys. Chem.*, 1960, **64**, 188–190.
44 M. J. Frisch, G. W. Trucks, H. B. Schlegel, G. E. Scuseria, M. A. Robb, J. R. Cheeseman, G. Scalmani, V. Barone, G. A. Petersson, H. Nakatsuji, X. Li, M. Caricato, A. V. Marenich, J. Bloino, B. G. Janesko, R. Gomperts, B. Mennucci, H. P. Hratchian, J. V. Ortiz, A. F. Izmaylov, J. L. Sonnenberg, D. Williams-Young, F. Ding, F. Lipparini, F. Egidi, J. Goings, B. Peng, A. Petrone, T. Henderson, D. Ranasinghe, V. G. Zakrzewski, J. Gao, N. Rega, G. Zheng, W. Liang, M. Hada, M. Ehara, K. Toyota, R. Fukuda, J. Hasegawa, M. Ishida, T. Nakajima, Y. Honda, O. Kitao, H. Nakai, T. Vreven, K. Throssell, J. A. Jr., J. E. Peralta, F. Ogliaro, M. J. Bearpark, J. J. Heyd, E. N. Brothers, K. N. Kudin, V. N. Staroverov, T. A. Keith, R. Kobayashi, J. Normand, K. Raghavachari, A. P. Rendell, J. C. Burant, S. S. Iyengar, J. Tomasi, M. Cossi, J. M. Millam, M. Klene, C. Adamo, R. Cammi, J. W. Ochterski, R. L. Martin, K. Morokuma, O. Farkas, J. B. Foresman and D. J. Fox, Gaussian, Inc., Wallingford CT (2016) *GaussView 5.0*. Wallingford, E.U.A.
45 J. Tomasi, B. Mennucci and R. Cammi, *Chem. Rev.*, 2005, **105**, 2999–3094.
46 A. D. Becke, *J. Chem. Phys.*, 1993, **98**, 5648–5652.
47 C. Lee, W. Yang and R. G. Parr, *Phys. Rev. B.*, 1988, **37**, 785.

48 W. Küchle, M. Dolg, H. Stoll and H. Preuss, *J. Chem. Phys.*, 1994, **100**, 7535–7542.
49 T. H. Dunning Jr., *J. Chem. Phys.*, 1989, **90**, 1007–1023.
50 K. Stanistreet-Welsh and A. Kerridge, *Phys. Chem. Chem. Phys.*, 2023, **25**, 23753–23760.
51 C. A. Andersson and R. Bro, *Chemom. Intell. Lab. Syst.*, 2000, **52**, 1–4.
52 B. Drobot, R. Steudtner, J. Raff, G. Geipel, V. Brendler and S. Tsushima, *Chem. Sci.*, 2015, **6**, 964–972.
53 S. M. Gutenthaler, S. Tsushima, R. Steudtner, M. Gailer, A. Hoffmann-Röder, B. Drobot and L. J. Daumann, *Inorg. Chem. Front.*, 2022, **9**, 4009–4021.
54 B. Drobot, M. Schmidt, Y. Mochizuki, T. Abe, K. Okuwaki, F. Brulfert, S. Falke, S. A. Samsonov, Y. Komeiji, C. Betzel, T. Stumpf, J. Raff and S. Tsushima, *Phys. Chem. Chem. Phys.*, 2019, **21**, 21213–21222.
55 C. W. Davies, *Ion Association*, Butterworths, London, 1962.
56 H. Moll, A. Rossberg, R. Steudtner, B. Drobot, K. Müller and S. Tsushima, *Inorg. Chem.*, 2014, **53**, 1585–1593.
57 W.-S. Jung, M. Harada, H. Tomiyasu and H. Fukutomi, *Bull. Chem. Soc. Jpn.*, 1988, **61**, 3895–3900.
58 G. R. Choppin and L. F. Rao, *Radiochim. Acta*, 1984, **37**, 143–146.
59 B. Drobot, A. Bauer, R. Steudtner, S. Tsushima, F. Bok, M. Patzschke, J. Raff and V. Brendler, *Anal. Chem.*, 2016, **88**, 3548–3555.
60 C. Lucks, Ph.D., Technische Universität Dresden, 2012.
61 S. Berto, F. Crea, P. G. Daniele, C. De Stefano, E. Prenesti and S. Sammartano, *Radiochimica Acta*, 2012, **100**, 13–28.
62 A. Kirishima, T. Kimura, O. Tochiyama and Z. Yoshida, *J. Alloys Compd.*, 2004, **374**, 277–282.
63 I. Feldman, J. R. Havill and W. F. Neuman, *J. Am. Chem. Soc.*, 1954, **76**, 4726–4732.